

Subharmonic Shapiro steps of sliding colloidal monolayers in optical lattices

Stella V. Paronuzzi Ticco^{1,2}, Gabriele Fornasier¹, Nicola Manini^{1,2}, Giuseppe E. Santoro^{2,3,4}, Erio Tosatti^{2,3,4}, and Andrea Vanossi^{2,3}

¹ Dipartimento di Fisica and CNR-INFM, Università di Milano, Via Celoria 16, 20133 Milano, Italy

² International School for Advanced Studies (SISSA), Via Bonomea 265, I-34136 Trieste, Italy

³ CNR-IOM Democritos National Simulation Center, Via Bonomea 265, 34136 Trieste, Italy

⁴ International Center for Theoretical Physics (ICTP), P.O.Box 586, I-34014 Trieste, Italy

E-mail: nicola.manini@fisica.unimi.it

Abstract. We investigate theoretically the possibility to observe dynamical mode locking, in the form of Shapiro steps, when a time-periodic potential or force modulation is applied to a two-dimensional (2D) lattice of colloidal particles that are dragged by an external force over an optically generated periodic potential. Here we present realistic molecular dynamics simulations of a 2D experimental setup, where the colloid sliding is realized through the motion of soliton lines between locally commensurate patches or domains, and where the Shapiro steps are predicted and analyzed. Interestingly, the jump between one step and the next is seen to correspond to a fixed number of colloids jumping from one patch to the next, across the soliton line boundary, during each AC cycle. In addition to ordinary “integer” steps, coinciding here with the synchronous rigid advancement of the whole colloid monolayer, our main prediction is the existence of additional smaller “subharmonic” steps due to localized solitonic regions of incommensurate layers executing synchronized slips, while the majority of the colloids remains pinned to a potential minimum. The current availability and wide parameter tunability of colloid monolayers makes these predictions potentially easy to access in an experimentally rich 2D geometrical configuration.

PACS numbers: 82.70.Dd,83.85.Vb,68.35.Af

1. Introduction

Driven nonlinear systems can show widely intriguing patterns of varied and often unexpected dynamical behavior. An especially interesting case is that of many identical interacting and crystallized particles moving in a periodic external potential: a common situation, e.g. for adatom structures sliding on a crystalline surface. In the special case when, besides the main time-independent force which causes the sliding, an additional external "AC" force component is present and oscillates periodically in time, synchronization phenomena are known to occur, depending on the relative importance of the interactions and on the geometrical arrangement of the particles.

Synchronization phenomena of this kind have long been described using simple, low-dimensional, phenomenological models, which often suffice to capture the main features of the complex dynamics involved. The basic example is provided by the simple yet fundamental one-dimensional (1D) Frenkel-Kontorova (FK) chain model [1, 2, 3] whose soliton, or kink pattern is known to exhibit a nontrivial intermittent dynamics, when additional time-periodic forces act on the otherwise steadily sliding chain [4]. This simple 1D model however is not generally sufficient to describe in full the complex dynamics of atoms at the interface of two materials in relative motion. Experimental studies of two-dimensional (2D) arrays of mutually repelling colloids pushed across a periodic "corrugation" potential landscape have recently been carried out, providing a closer analog of the sliding of crystalline interfaces [5, 6, 7, 8]. Before sliding, the observed 2D patterns of misfit dislocation lines (referred to as solitons or kinks) are very much akin to the Moiré patterns formed by atomic overlayers over crystal surfaces. Besides their surface physics analog, the colloid systems have an interest on their own because they provide a ready parameter-controlled system for the study of friction between crystalline surfaces [9, 7, 10].

Here we explore, ahead of experiments, just very recently available in a simpler 1D geometry [11], a situation where synchronization, whence the existence and the actual dynamical nature of Shapiro steps, is sought by oscillating in time either the pushing force or the amplitude of the (x, y) periodic corrugation potential. In particular we focus on the second, corresponding to an ideal setup where colloids thread a partially time-modulated spatially-periodic optical potential, and investigate in particular the effects of the mismatch between the colloid-colloid average spacing of the 2D colloid crystal and the periodicity of the optical potential.

Shapiro steps were initially observed [12] in the context of Josephson junctions. The crucial ingredient at the start was Josephson's prediction [13] of a coherent current $I_c \sin \phi$ flowing between two superconductors separated by a thin insulating barrier in presence of a phase difference $\phi = \phi_1 - \phi_2$ between the two superconductor order parameters. Moreover, a potential difference $V = \frac{\hbar}{2e} \frac{d\phi}{dt}$ was predicted to be associated to a phase ϕ that changes in time, with the remarkable consequence, known as AC Josephson effect, that the coherent current would oscillate with a frequency $\omega_0 = 2eV_{dc}/\hbar$ in presence of a constant DC bias V_{dc} . The fingerprint of ω_0 can be

detected through an ingenious resonance experiment [12], in which a current $I(t) = I_{\text{dc}} + I_{\text{ac}} \sin(\omega t)$ is passed through the junction. A simple model [14, 15] capturing resistive and capacitive effects in the junction would allow us to write:

$$\frac{\hbar C}{2e} \frac{d^2 \phi}{dt^2} + \frac{\hbar}{2eR} \frac{d\phi}{dt} + I_c \sin \phi = I(t), \quad (1)$$

where C is the capacitance of the junction, and $\frac{\hbar C}{2e} \frac{d^2 \phi}{dt^2} = C \frac{dV}{dt}$ the corresponding current, while $\frac{\hbar}{2eR} \frac{d\phi}{dt} = \frac{V}{R}$ accounts for the resistive part of the current, due to quasi-particles. In general, a $\phi(t) = \omega_0 t + \Delta_\phi(t)$ where $\Delta_\phi(t)$ is a bounded function, implies a (time-averaged) DC voltage $V_{\text{dc}} = \frac{\hbar \omega_0}{2e}$ across the junction. In a non-resonant situation, $\sin \phi(t)$ oscillates in an aperiodic way with zero average, $\langle \sin \phi(t) \rangle_{\text{time}} = 0$; hence the (time-averaged) DC voltage predicted by Eq. (1) follows the usual Ohmic I-V characteristics, $V_{\text{dc}} = R I_{\text{dc}}$. Resonances instead can make $\langle \sin \phi(t) \rangle_{\text{time}} \neq 0$ by the following phase-locking mechanism [16]: the bounded variation $\Delta_\phi(t)$ becomes a periodic function of time, characterized by the frequency ω of the external driving, while the slope of $\phi(t)$ — the frequency ω_0 — exactly matches a multiple of the driving frequency ω : $\omega_0 = n\omega$. In such resonant situations, $\sin \phi(t)$ becomes periodic and with non-zero average, $\langle \sin \phi(t) \rangle_{\text{time}} \neq 0$, implying that the constant terms in Eq. (1) obtained by averaging over a period sum up to:

$$\frac{V_{\text{dc}}}{R} + I_c \langle \sin \phi(t) \rangle_{\text{time}} = I_{\text{dc}}. \quad (2)$$

In essence, at resonances, I_{dc} can be changed by an amount $\sim I_c \langle \sin \phi(t) \rangle_{\text{time}}$ without affecting the voltage bias V_{dc} : these are the *Shapiro steps* in the I-V characteristics, where the the voltage step is strictly quantized through a finite range of current.

A mechanical analogy of the Josephson junction model of Eq. (1) is straightforward, with the phase difference $\phi(t)$ playing the role of a coordinate $x(t)$, the voltage $V \propto d\phi/dt$ that of the velocity of a particle moving in a washboard potential, and the current $I(t)$ the role of an external force. Shapiro steps have then a natural translation into “quantized” steps of the velocity of the moving particle for a finite range of applied force, when the washboard frequency goes in resonance with the AC perturbing frequency ω . This resonance phenomenon is robust, and one could for instance periodically modulate the amplitude of the space-periodic corrugation potential [the analog of I_c in Eq. (1)] rather than the external force, and the same physics would follow.

As is shown in Eq. (1), the Shapiro physics involves a single degree of freedom. However, in systems of many interacting particles, crystallized but not rigid, synchronization phenomena of the Shapiro kind are likely to give rise to additional nontrivial dynamical effects due to concerted multi-particle motion. The strong interest in synchronization phenomena in multiple physical contexts has generated numerous research works in recent years, among which we recall Refs. [11, 17, 18, 19, 20, 21, 22, 23, 24, 25]. The system where we propose to explore the Shapiro physics consists of a collection of repulsive colloidal particles dragged by an external force over a spatially periodic corrugation potential, whose amplitude includes both a static and a time-oscillating part. When the frequency ω of the oscillation is a multiple of the characteristic

(washboard) frequency ω_0 , the forced sliding motion of the 2D colloid lattice can give rise to Shapiro steps. Combined experimental and simulation studies already addressed in the past the effect of synchronization and the ensuing Shapiro steps in Brownian particle dynamics [24]. Other simulation work [26] addressed the case where the 2D sliding lattice and the periodic potential are fully matched, in addition to ratcheting conditions in mixtures. Very recently, the microscopic dynamics underlying mode locking in a colloidal model system has been recorded in a simple, yet noteworthy, 1D experimental setup [11]. In this work we study the feasibility of observing Shapiro steps under reasonably realistic conditions in 2D sliding colloid monolayers, under the wider range of conditions that can be realized experimentally. More specifically, we will describe a planar system of monodisperse repulsive particles, forming a 2D triangular lattice with spacing a_{coll} , sliding within a periodic corrugation potential due to an optical lattice, also triangular with spacing a_{las} , whose amplitude is partly modulated periodically in time, under various conditions as determined by different choices of the commensurability ratio $\rho = a_{\text{las}}/a_{\text{coll}}$. Using classical molecular dynamic we will monitor the individual motion of the particles as well as that of their center of mass (CM) under the action of a DC force. As a function of this force the forward CM velocity of the colloidal particles should, owing to Shapiro synchronization, become 'quantized' in step-like structures as a function of the applied force. Our aim is therefore to seek, detect and characterize these step structures in relation to the absence (in the fully matched, commensurate case $\rho = 1$) or presence, e.g., for $\rho < 1$ of pre-existing soliton-like defects or kinks due to mismatched relative spacings of the colloidal lattice and of the periodic potential.

2. The model

Molecular dynamics (MD) simulations are based on the same model already introduced [10] to describe the motion of mutually repulsive charged colloidal particles driven across a periodic potential generated by a light interference pattern, as realized in experiments by Bohlein *et al.* [7, 8]. In short, we describe the charged colloidal particles as classical point-like objects, whose dynamics is affected by their mutual repulsion, the action of external forces, plus the interaction with the viscous fluid where they are immersed.

The equation of motion for the j -th particle is

$$m\ddot{\mathbf{r}}_j(t) + \eta(\dot{\mathbf{r}}_j(t) - v_d\hat{\mathbf{x}}) = -\nabla_{\mathbf{r}_j}(U_2 + U_{\text{ext}}) + \mathbf{f}_j(t), \quad (3)$$

where \mathbf{r}_j is the position of the j -th colloid in the 2D plane where it can move, η is the friction coefficient determined by the effective viscosity of the fluid in which the colloids are immersed, and v_d is the fluid drift velocity, giving rise to a Stokes driving force $F = \eta v_d$, pushing forward all colloidal particles. U_2 is the two-body inter-particle potential; U_{ext} is the corrugation potential describing the interaction with the spatially periodic light-field pattern. In this work we especially focus on the effect of time-periodic oscillations of the amplitude of U_{ext} . The finite-temperature Brownian motion of colloids is introduced in a standard Langevin approach, involving the viscous friction

ρ	η	N	N_{minima}	Q	λ_D	L_x	L_y
1	28	392	392	10^{13}	0.03	14	$14\sqrt{3}$
14/15	28	392	450	10^{13}	0.03	14	$14\sqrt{3}$
3/4	28	450	800	10^{13}	0.03	15	$15\sqrt{3}$

Table 1: Adopted simulation parameters, expressed in model units [10]. For example, the simulation-cell sides L_x and L_y are given in units of the average colloid lattice spacing a_{coll} . N_{minima} is the number of identical local minima of the corrugation function $W(\mathbf{r})$ contained in a simulation cell.

term $\eta(\dot{\mathbf{r}}_j(t) - v_d \hat{\mathbf{x}})$, plus the Gaussian random force $\mathbf{f}_j(t)$ [27]. Due to the low overall velocity ($v_d \simeq 10 \mu\text{m s}^{-1}$) of the colloidal particles, the inertial term can be neglected, and an overdamped diffusive motion is reasonably assumed, with a sufficiently large η . In our work $\eta = 28$ expressed in the same model units described in Ref. [10]. Typical simulation parameters are reported in Table 1.

The two-body interaction potential is

$$U_2 = \sum_{j < j'}^N V_{\text{Yuk}}(|\mathbf{r}_j - \mathbf{r}_{j'}|), \quad (4)$$

where the screened Coulomb repulsion V is a Yukawa potential:

$$V_{\text{Yuk}}(r) = \frac{Q}{r} \exp(-r/\lambda_D). \quad (5)$$

The average nearest-neighbor separation of colloids in Ref. [7] is $r = a_{\text{coll}} \simeq 5.7 \mu\text{m} \simeq 30\lambda_D$. Under confinement, this repulsion establishes a triangular lattice of colloids, which can be thought as reasonably defect free at temperatures not too high and sizes sufficiently small to render the possibility of Nelson-Halperin dislocations [28] irrelevant to the present case.

The one-body term

$$U_{\text{ext}} = \sum_j^N V_{\text{ext}}(\mathbf{r}_j, t), \quad (6)$$

describes the interaction of the colloids with the 2D spatially periodic potential, representing the optical lattice corrugation. Its actual form, determined by $V_{\text{ext}}(\mathbf{r})$, could in principle be shaped with some freedom, but the simplest sinusoidal form is sufficient to describe the main phenomena. We thus take:

$$V_{\text{ext}}(\mathbf{r}, t) = [V_0 + \Delta_0 \sin(\omega t)] W(\mathbf{r}), \quad (7)$$

where

$$W(\mathbf{r}) = -\frac{1}{9} \left[3 + 4 \cos\left(\frac{2\pi r_y}{\sqrt{3} a_{\text{las}}}\right) \cos\left(\frac{2\pi r_x}{a_{\text{las}}}\right) + 2 \cos\left(\frac{4\pi r_y}{\sqrt{3} a_{\text{las}}}\right) \right], \quad (8)$$

a unit-amplitude eggcarton-type periodic potential of 6-fold symmetry representing the optical-lattice triangular corrugation. The time-dependent amplitude $V_0 + \Delta_0 \sin(\omega t)$

gives to the corrugation an additional sinusoidal time dependence that can induce synchronization effects. Its amplitude $2\Delta_0$ yields a total corrugation ranging between $V_0 - \Delta_0$ and $V_0 + \Delta_0$ with an AC modulation frequency $\nu = \omega/(2\pi)$. The minimum force required to dislodge an isolated colloid at $T = 0$ along direction x is at time t

$$F_{s1} = \frac{8\pi}{9} \frac{V_0 + \Delta_0 \sin(\omega t)}{a_{\text{las}}}. \quad (9)$$

The quantity $8V_0/(9a_{\text{las}})$ is used as our unit of force. In general, the spacing a_{las} of the corrugation lattice potential $W(x, y)$ can be tuned in such a way to be either matched or mismatched with the colloidal lattice. In mismatched configurations, one observes, both in simulations [10] and in experiments [7], the formation of misfit dislocations also called *topological solitons*, or kinks/antikinks in the language of the FK model [29]. Their existence and their motion under the external force dominates the frictional properties of the sliding lattice, since it provides the mechanism for mass transport [30].

As for the oscillation frequency, it needs to be low enough for the overdamped colloidal system to be allowed enough time to follow adiabatically the AC modulation in the corrugation-amplitude oscillation. The specific condition is $\nu \ll \eta/m$, and we use $\nu < 0.1$ in model units. Shapiro-step structures can arise out of synchronization of the washboard frequency ω_0 of the colloids driven by F over the corrugation potential, with the time-modulation frequency ω of Eq. (7). At finite temperature (e.g. in experimental conditions), ν must also not to be so small that particle random diffusion overshadows the ordered synchronized crossing of potential energy barrier.

Our protocol begins with a preliminary relaxation preparing the sample in its equilibrium, force-free initial state. Sliding simulations are then conducted by applying a force $F = \eta v_d$ along x on each particle, similar to the viscous drag of the flowing fluid in experiments. The static force F is slowly ramped upwards in small steps ΔF , so as to explore the desired force range. At each force value, after an initial transient lasting between 1 and 10 oscillation periods, the particle CM displacement Δx_{cm} is extracted for the successive simulation time τ , typically a large integer (of order 100) number of periods ν^{-1} of the time-dependent perturbation. We then record the average speed $v_{\text{cm}} = \Delta x_{\text{cm}}/\tau$ for each value of the driving force F .

Experimental conditions [7] actually involve an inhomogeneous 2D configuration, whereby only a circular central portion of the colloid monolayer raft is submitted to the laser field with its associated optical lattice potential. However, only phenomena in the central part of this circle are eventually studied, and there the colloids are virtually homogeneous. Therefore, we conduct the present study in a fully homogeneous 2D colloid lattice with periodic boundary conditions (PBC) qualitatively represented in Fig. 1. Given a cell size and a particle number, we will simulate either the commensurate and fully matched geometry ($\rho = 1$), or mismatched underdense geometries ($\rho < 1$), by tuning appropriately the corrugation lattice spacing a_{las} relative to that of the colloid lattice, a_{coll} .

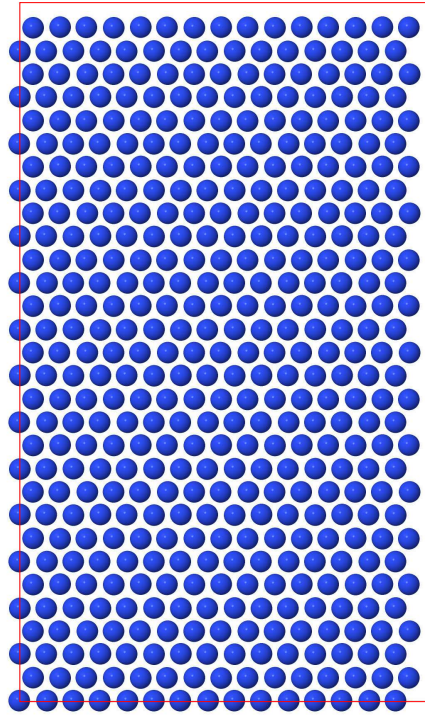


Figure 1: The $L_x \times L_y = 15 a_{\text{coll}} \times 15\sqrt{3} a_{\text{coll}}$ rectangular simulation cell (solid line) adopted for the $\rho = 3/4$ simulations. In this initial snapshot, the 450 particles still form a perfect triangular lattice.

3. Perfect lattice matching

We begin with the fully matched commensurate geometry where, at $\rho = 1$, the two triangular lattices coincide, and no preliminary relaxation is needed, each particle falling in a potential minimum. We then turn on the sliding force with a time-dependent modulation of amplitude $\Delta_0 = 40\% V_0$, with an intermediate corrugation strength $V_0 = 0.5$, at $T = 0$. The average CM velocity as a function of the external force F is presented in Fig. 2. As a function of the sliding force, it shows Shapiro steps, i.e. plateaus in the average CM velocity. These steps correspond to integer multiples of νa_{las} in the force-velocity response. In these $T = 0$ simulations the motion of the colloids is deterministic, leading to perfectly flat steps with null error bars, as long as the CM speed is averaged over an integer number of periods ν^{-1} . The reference velocity νa_{las} is that of a particle advancing by one corrugation spacing a_{las} in one oscillation period ν^{-1} . Depending on the applied DC force, all particles advance together by an integer number of lattice spacings a_{las} at each period of the AC modulation. As a function of ν both the velocity jump between successive Shapiro steps, and the force step width increase proportionally to ν , as expected. Correspondingly, the number of steps in a given force range decreases for increasing ν . In the large force regime, for $F > \frac{8\pi}{9} (V_0 + \Delta_0)/a_{\text{las}} \simeq 1.95$, the steps rapidly decrease in width, and merge into a

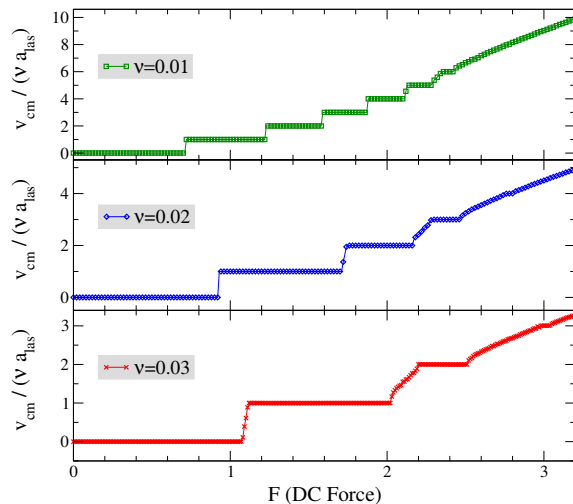


Figure 2: $T = 0$ Shapiro steps observed in the CM velocity parallel to the applied force obtained for a fully commensurate colloid lattice ($a_{\text{las}} = a_{\text{coll}}$, $\rho = 1$) with a corrugation amplitude $V_0 = 0.5$, a modulation amplitude $\Delta_0 = 0.2$, for values of the frequency $\nu = 0.01, 0.02$, and 0.03 (in model units). The velocity is scaled by νa_{las} , to emphasize the proportionality of the exactly quantized steps to the modulation frequency.

smooth velocity increase proportional to force, characteristic of a viscous regime, similar to the non-modulated $\Delta_0 = 0$ dynamics [7, 10].

In this zero-temperature lattice-matched system, all colloids execute the same movement to negotiate the crossing of the same energy barriers. As a result, the colloid-colloid mutual spacing remains constant, and the colloid-colloid internal force does no work. The dynamics would be exactly the same if the colloidal particles were not interacting, or if the simulation involved one particle only, moving in the same potential-energy profile. As a check, we repeated the simulations with a single particle, indeed recovering exactly the same patterns as in Fig. 2.

We explore now how the AC modulation amplitude Δ_0 affects these Shapiro steps. Figure 3 shows the velocity curves obtained with the same average corrugation amplitude ($V_0 = 0.5$) and AC modulation amplitude rising from the same initial value $\Delta_0 = 40\% V_0$ as in the central panel of Fig. 2 ($\nu = 0.02$), to larger values $\Delta_0 = 70\% V_0$ and $\Delta_0 = 100\% V_0$, at the same frequency. For larger Δ_0 the colloid system starts to move earlier, i.e., at a smaller DC force than for a smaller Δ_0 . Note that at 100% relative modulation amplitude, every oscillation period has a brief instant where the colloid layer actually slides freely. Despite this free-sliding instant, the force needed for the monolayer to depin and reach the first Shapiro step, even though smaller than at 40% modulation amplitude, appears anyway to be nonzero. The reason for that is the finite time it takes the colloid to drift across the momentarily turned off barrier to the next substrate minimum, when the driving force F is small. This issue is discussed in detail in Sect. 5 below.

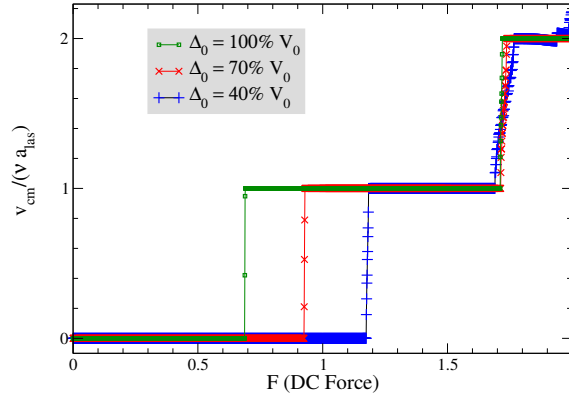


Figure 3: Shapiro steps for $\nu = 0.02$, $V_0 = 0.5$, for increasing AC modulation amplitude Δ_0 . Pluses: $\Delta_0 = 40\% V_0$, same as in the central panel of Fig. 2. Crosses: $\Delta_0 = 70\% V_0$. Squares: $\Delta_0 = 100\% V_0$. The step heights are unchanged, their widths increase, and the jump between successive steps becomes steeper for increasing Δ_0 .

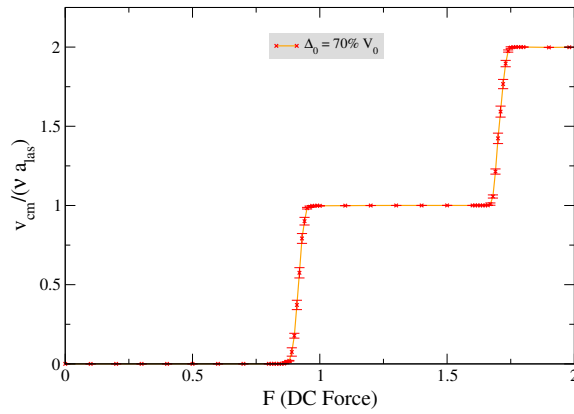


Figure 4: Finite-temperature Shapiro-step structure for a fully commensurate system. Temperature $T = T_{\text{room}}$, and the other simulation conditions ($\nu = 0.02$, $V_0 = 0.5$, $\Delta_0 = 70\% V_0$) are the same as for the crosses data of Fig. 3. The effect of thermal motion is barely detectable, apart from a slight rounding on the step edges. Thermal fluctuations of the CM velocity, reflected by the error bars, are visible at rises between steps, but negligible inside the steps.

3.1. Thermal effects

So far we worked at $T = 0$, because that regime yields a clearer picture. Next, however, we can ask how the Shapiro steps might be affected by thermal fluctuations in the experimental, room-temperature conditions. To address this question, we perform new simulations at room temperature $T = T_{\text{room}}$ ($T_{\text{room}} = 0.04$ in system units), still at $\rho = 1$ and keeping all other parameters (mimicking the experimental colloid system of Ref. [7]) the same. Figure 4 shows that the Shapiro-step structure is barely affected; T_{room} is a very moderate temperature for this system. Thermal fluctuations (estimated by the standard deviation of v_{cm} obtained over several sliding simulations realized with

independent random-number sequences and different initial configurations ensuring a better sampling of the thermal equilibrium state) are visible, as reflected by the error bars, at jumps between steps. Thermal fluctuations produce a rounding of the plateau onset, but are barely visible inside each plateau.

4. Mismatched lattice spacing

When the commensurability ratio $\rho = a_{\text{las}}/a_{\text{coll}}$ differs from unity the colloid and the corrugation lattices are mismatched. As we shall see, in this case the internal structure of the sliding lattice plays a role, and the expected Shapiro-step phenomena become more interesting. It must be clarified at the outset that the Shapiro steps exist only if the system is pinned by a finite static friction force. For example, a 2D colloid lattice incommensurate with a weak periodic corrugation is an unpinned system which can slide “superlubrically” without static friction, and will exhibit no Shapiro steps. The same incommensurate lattice must however become pinned when the corrugation amplitude exceeds a first-order depinning-pinning transition threshold value [31], and here Shapiro steps can exist. This is the situation which we concentrate upon here. We describe in detail two different examples of mismatched configurations, $\rho = 14/15 \simeq 0.93$ and $\rho = 3/4 = 0.75$. Both are *underdense* systems compared to the perfectly matched one with $\rho = 1$ considered in Sec. 3, and both are of course rationally commensurate. However, the commensurability of $\rho = 3/4$ is so to speak stronger, that in $\rho = 14/15$ weaker, the latter case in a sense closer to incommensurability, itself a condition impossible to reach in a finite-size PBC realization. We will further assume that the colloids and the corrugation lattice do not undergo a relative rotation, e.g., of the type studied in Refs. [32, 33, 34, 35, 36], and therefore remain aligned. With that stipulation we adopt for $\rho = 14/15$ a rectangular periodic simulation cell involving 392 colloids threading 450 corrugation potential minima. With 14 colloidal particles threading 15 potential wells along each principal direction, we obtain a widely spaced hexagonal network of misfit dislocation lines (*antisolitons*), where vacancies segregate. Details of this case will be shown later. For $\rho = 3/4$ we also adopt a rectangular supercell, here involving 450 colloids and 800 potential minima, shown in Fig. 1. The higher vacancy concentration leads to a greater mismatch and therefore a denser packing of antisolitons.

In these mismatched systems we must first of all identify the corrugation amplitude at which, as was mentioned above, a pinning/depinning transition takes place in the absence of AC modulation ($\Delta_0 = 0$). In the limit of infinitesimal applied force, this transition was recently discovered and characterized by Mandelli *et al.* [31]. Ignoring here the weak 14/15 commensurability and taking this to represent a truly incommensurate case, this is the 2D analog of the celebrated 1D “Aubry transition” [29, 38, 31] here taking place at $V_{0\text{crit}} \simeq 0.4$ [39]. With this stipulation, for every corrugation value $V_0 < V_{0\text{crit}}$ the colloid sliding over the incommensurate corrugation is “superlubric”, and will take place for arbitrarily small applied force. By contrast, when

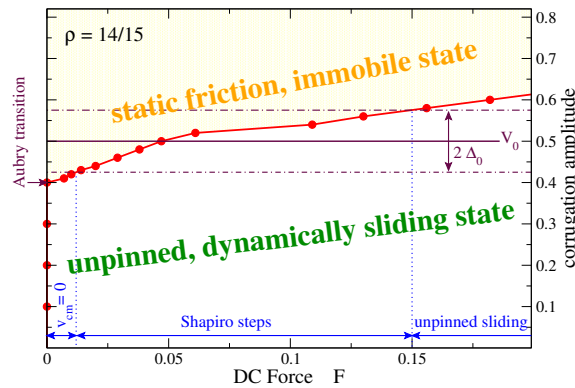


Figure 5: DC Force F – corrugation amplitude V_0 phase diagram for $\rho = 14/15$ mismatched colloids, in the absence of AC modulation ($\Delta_0 = 0$). The red dots and line represent the depinning line where at $T = 0$ the colloid abandons the statically pinned state (shaded yellow region) in favor of a (nearly) free-sliding state for larger force F . A truly incommensurate monolayer, where ρ is irrational, would exhibit a very similar transition line, the 2D analogue of the 1D Aubry transition [31, 37]. Horizontal solid and dot-dashed lines: a choice of corrugation ($V_0 = 0.5$) and AC modulation $\Delta_0 = 15\% V_0$ amplitudes. In the force range for which both dot-dashed lines are in the shaded region, the colloid layer is pinned. For large force, when both dot-dashed lines lie below the depinning curve, the colloids advance freely. The intermediate force interval is the one affected by the synchronization to the AC potential modulation, giving rise to Shapiro steps.

$V_0 > V_{0\text{crit}}$, the monolayer is pinned, and a finite static friction force $F > 0$ is required to make the system slide [31]. The curve of Fig. 5 represents precisely this depinning transition line for the $\rho = 14/15$ mismatched system, for nonzero and increasing force.

To understand what happens when we superpose an AC corrugation modulation $\Delta_0 > 0$ to the “phase diagram” of Fig. 5, we add horizontal dot-dashed lines representing the maximum and minimum value covered by the overall corrugation magnitude during an oscillation. As an example, in Fig. 5 we sketch $V_0 = 0.5$ (horizontal solid line) and $\Delta_0 = 15\% V_0$ (horizontal dot-dashed lines). Synchronization between the washboard sliding frequency and the AC modulation, and consequently Shapiro steps, can arise naturally in the intermediate range of forces $0.02 \leq F \leq 0.15$, where at each modulation period the system crosses twice the pinned-unpinned transition curve. Figure 5 shows that depending on V_0 and Δ_0 , the F dependence can vary quite substantially. For example, if $V_0 + \Delta_0 < V_{0\text{crit}}$, then for any F the colloids will slide freely. For $V_0 + \Delta_0 > V_{0\text{crit}}$ but $V_0 - \Delta_0 < V_{0\text{crit}}$ the initial pinned region ($F \leq 0.02$ in figure) would disappear: in this case the first Shapiro step could extend to arbitrarily small applied force, by reducing the modulation frequency ν , as further discussed in Sec. 5. This phase diagram can be taken as a guide for the choice of the simulation parameters. In order to observe Shapiro steps, the colloid lattice must be pinned, e.g., V_0 must be above the critical corrugation $V_{0\text{crit}}$. The range of force where Shapiro steps exist widens

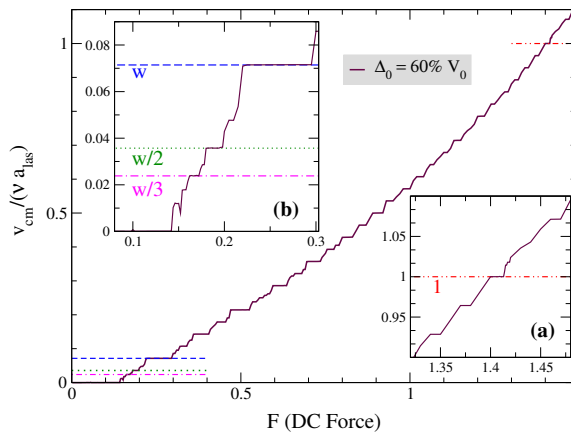


Figure 6: The Shapiro-step structure of the lattice mismatched $\rho = 14/15$ configuration simulated at $T = 0$, with corrugation amplitude $V_0 = 1$, modulation $\Delta_0 = 60\% V_0$, and AC frequency $\nu = 0.02$. (a) A zoom-in of the region of the “trivial” commensurate step $v_{\text{cm}}/(\nu a_{\text{las}}) = 1$ corresponding to all colloids advancing by a_{las} at each period. (b) A zoom-in of the region of the subharmonic steps, highlighting those matching $w = |1 - \rho^{-1}| = 1/14$ and integer submultiples thereof.

out as the modulation amplitude Δ_0 is increased. The phase diagram for $\rho = 3/4$ is quite similar to that of $\rho = 14/15$, and in particular $V_{0,\text{crit}} \simeq 0.42$ is nearly the same.

We now explore and describe the existence and nature of Shapiro steps in these mismatched cases, adopting an arbitrary but reasonable corrugation $V_0 = 1 > V_{0,\text{crit}}$ and AC modulation $\Delta_0 = 60\% V_0$ (different parameters were explored too). Unlike the $\rho = 1$ case, here a preliminary and careful relaxation of the initial force-free, equilibrium structure is required. An initial simulation for a duration $\tau = 1000$ is thus performed with a time-independent corrugation (V_0 turned on, $\Delta_0 = 0$), and no external force applied ($F = 0$). Starting from the relaxed configuration, a sequence of force-driven sliding simulations is run, now with the AC corrugation modulation turned on.

4.1. $\rho = 14/15$

4.1.1. Step structure. Let us consider $\rho < 1$, where it is useful to introduce as a misfit measure the quantity

$$w = \left| 1 - \frac{a_{\text{coll}}}{a_{\text{las}}} \right| = \left| 1 - \frac{1}{f} \right|, \quad (10)$$

This quantity was found earlier to be the relevant parameter in the context of simulations of mismatched crystalline systems in mutual contact, Refs. [40, 41, 42, 43, 44, 45, 46, 47, 48, 49, 50, 51]. The results of sliding simulation for $w = 1/14$, corresponding to $\rho = 14/15$, are shown in Fig. 6. The Shapiro steps exist here too, but the mismatched geometry exhibits a far richer pattern of Shapiro steps than the lattice-matched case: we detect tens of steps in a much narrower force range than in the commensurate case of Fig. 2.

First off, the regular integer plateau at $v_{\text{cm}}/(\nu a_{\text{las}}) = 1$, at the same speed as the first step in fully matched geometry, Fig. 3, is detailed in the inset Fig. 6a. Additionally, Fig. 6 exhibits several other subharmonic steps at smaller driving force. It has long been known that for mismatched lattices also *fractional subharmonic Shapiro plateaus*, i.e. plateau velocities which are not integer multiples of νa_{las} [4, 52] are to be expected. In particular the inset Fig. 6b zooms around a much lower speed, given by

$$\frac{v_{\text{cm}}}{\nu a_{\text{las}}} = w. \quad (11)$$

Here $w = 1/14$ and velocity steps appear at wm/n for several m and n values. All these $v_{\text{cm}} < \nu a_{\text{las}}$ plateaus are subharmonic Shapiro steps. Unlike in the integer plateaus, where all N particles advance by one (or several) lattice spacing(s) a_{las} in one period ν^{-1} , at a fractional plateau characterized by $v_{\text{cm}}/(\nu a_{\text{las}}) = wm/n$, a total fraction mwN of all colloids advances by one lattice spacings during n modulation periods.

The quantization of sliding velocity to the value of Eq. (11) was discovered and studied in the context of the sliding of mismatched crystalline systems in mutual contact, and reported in the study of two sliding surfaces with an atomically thin solid lubricant layer in between [40, 41, 42, 43, 44, 45, 46, 47, 48, 49, 50, 51]. There, the ratio ρ was that of the lattice spacing of a “bottom” slider to that of the lubricant layer, w was the mean velocity at which the lubricant moved over the bottom slider, in units of the externally imposed speed of the “top” slider. The sliding of the lubricant with relative speed w arose in that case because the vacancies (or interstitials) forming the antisolitons (solitons) were the real entities dragged forward at the full speed of the top layer, all (other) particles remaining essentially static. In the following we shall clarify the relationship between the driven soliton dynamics in the sliding-friction models and the subharmonic steps in the dynamics of colloids driven in a modulated-amplitude potential.

4.1.2. Subharmonically sliding antisolitons. Figure 7 shows that the antisoliton lines divide the cell into domains inside which the particles are essentially static at a minimum of the corrugation potential. The overall forward sliding motion demanded by the force F is actuated, for $\rho < 1$, through the backwards motion of the antisolitons, where all vacancies are lumped. The antisolitons move to the left in synchrony with the modulation, advancing faster when the instantaneous corrugation amplitude $V_0 + \Delta_0 \sin(\omega t)$ of Eq. (7) is minimum. At that moment a fraction of colloids jumps from the left to the right side of an antisoliton line, while all others remain essentially static. In the wm/n step, this colloid displacement results in the full antisoliton pattern moving by ma_{las} to the left every n modulation periods. Figure 8 illustrates the dynamics of a single colloid. Most of the time the particle just oscillates, following the AC modulation: when the amplitude $V_0 + \Delta_0 \sin(\omega t)$ is maximum, the particle is driven toward the nearest corrugation-potential well; when the amplitude is minimum, the particle relaxes due to the two-body repulsion. The amplitude of this oscillation is minimal when the colloid is near the center of a domain, Fig. 8c, and increases as the colloid reaches the antisoliton,

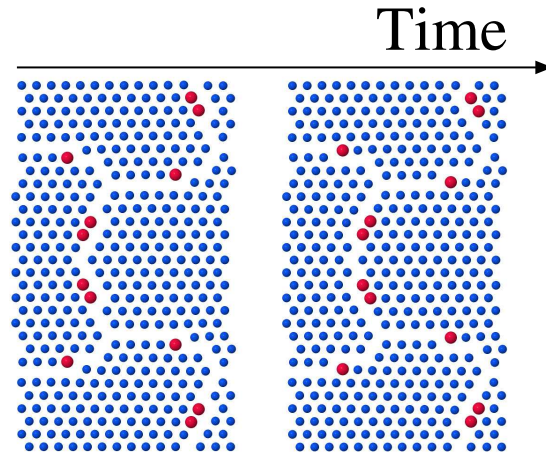


Figure 7: $\rho = 14/15$, $T = 0$, $w/3$ fractional plateau. The antisoliton pattern divides the colloid lattice into domains or patches inside which colloids are approximately matched to the static corrugation lattice. The underdense colloid monolayer slides rightward due to the leftward motion of the antisoliton line, while particles inside the domains do not slide. The specificity of this plateau is the behavior of particles at the antisoliton boundary. Left and right are two successive snapshots separated by a single oscillation period ν^{-1} . At the end of this time interval, most colloids still occupy their initial positions, but the 12 highlighted particles (red) crossed the antisoliton line to join the next commensurate domain to the right. In the two following ν^{-1} periods the remaining $Nw - 12 = 16$ particles will also cross, so that after the time $n\nu^{-1}$ (here with $n = 3$) all $Nw = 28$ particles will have crossed. Different plateaus with different w and different subharmonic n will have an analogous but different pattern of traversing particles.

which is the domain boundary. A positive, uncompensated velocity spike, see Fig. 8a,b, signals the moment when the particle crosses the gap and enters the neighboring domain, Fig. 8d,e. It should be noted here that some fraction of the colloid rightward motion also takes place while inside the commensurate domain, which is not rigid and thus becomes progressively deformed elastically.

We are now in a position to clarify the nature of the w subharmonic steps. To do this, we observe the colloidal pattern in a 'stroboscopic' approach, by comparing snapshots taken at successive times separated by one period, namely when the corrugation amplitude, Eq. (7), acquires its maximum value $V_0 + \Delta_0$, i.e. for successive half-odd integer values of νt . We highlight the particles that during the last period ν^{-1} have underwent a displacement exceeding a certain threshold δ . Due to the elastic domain deformations discussed above this threshold must be chosen appropriately: for the conditions considered here a value $0.12 a_{\text{coll}} \leq \delta \leq 0.61 a_{\text{coll}}$ provides consistent results for all plateaus. The highlighted particles represent colloids, whose number we designate as m_i , which cross the antisoliton boundary between two neighboring domains in that period i of oscillation. In the fundamental plateau where the quantized speed

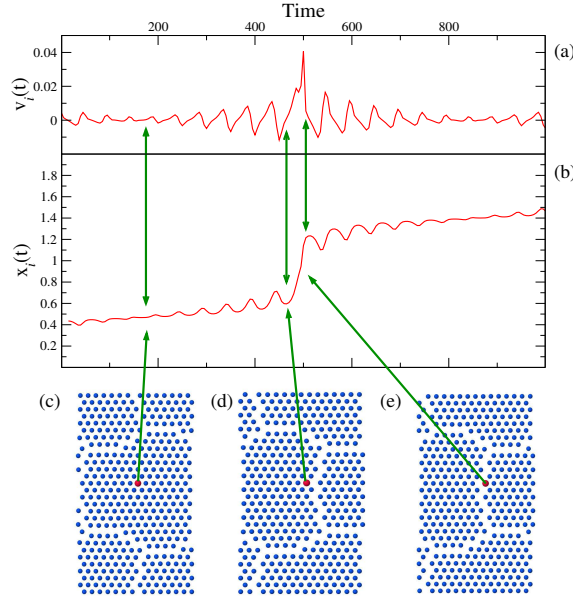


Figure 8: $\rho = 14/15$, $T = 0$: The time evolution of the x component of (a) velocity and (b) position of a single (highlighted in panels c-e) colloid, when $F = 0.24$ and the CM velocity is in the fractional Shapiro step of Fig. 6, characterized by $v_{\text{cm}}/(\nu a_{\text{las}}) = w = 1/14$. Because $\rho < 1$, the forward sliding motion is realized by a backward motion of vacancies, here forming antisoliton lines. Velocity shows alternating positive and negative spikes, plus a large positive peak when the leftward moving domain boundary reaches, between $t = 465$ and $t = 515$, the colloid, which then jumps across the antisoliton line, joining the next domain. Near the center of the domain – e.g. at $t \simeq 175$, panel (c) – the lateral oscillation amplitude reaches its minimum, because the particle sits close to a potential well bottom.

equals w , the pattern of advancing particles is the same at all oscillation periods, as seen, e.g., in Fig. 9 and equals Nw where N is the total number of particles. In the present case of Fig. 9 $N = 392$, $w = 1/14$, the Shapiro plateau has dimensionless velocity w , and a total of $Nw = 28$ particles cross the boundary to the next domain at each oscillation period. More specifically, 22 colloids at the edge of the island aligned along \hat{y} move straight in the \hat{x} direction into the next corrugation minimum at a distance a_{las} . In addition, 12 more particles along the oblique antisoliton line advance with a sideways \hat{y} component, thus proceeding into a minimum which is $a_{\text{las}}/2$ to the right. The total movement amounts therefore to effectively $22 + 12/2 = 28 = Nw$ particles advancing by a_{las} in each period. The very same picture applies to sliding a monolayer with any different lattice-spacing ratio $\rho = (1 + w)^{-1}$. The fundamental subharmonic step occurs again at velocity w .

The pattern of advancing colloids is somewhat more complex in the other subharmonic steps. We explore these differences in Figs. 9 and 10. To exemplify, let us consider again $w = 1/14$, but now focus on the $w/2$ plateau, Fig. 10. Here, a total

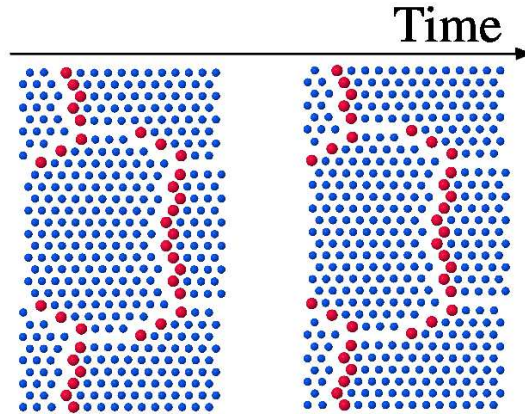


Figure 9: $\rho = 14/15$, $N = 392$ particles, $V_0 = 1$, forward force $F = 0.24$, step $w = 1/14$. Successive snapshot patterns of advancing colloids, separated by intervals of one oscillation period ν^{-1} . The antisolitons drift to the left, causing the CM to move to the right. The particles whose displacements exceed a fixed threshold δ are highlighted (lighter and bigger). In this step 22 particles shift to the right (i.e., along \hat{x}) in each oscillation period, crossing the vertical section of the antisoliton line, plus another 12 cross an oblique section, with a lateral \hat{y} component of motion, and only half distance along \hat{x} . As a result a total of $22 + 12/2 = 28$ particles advance by a_{las} , joining the next commensurate domain.

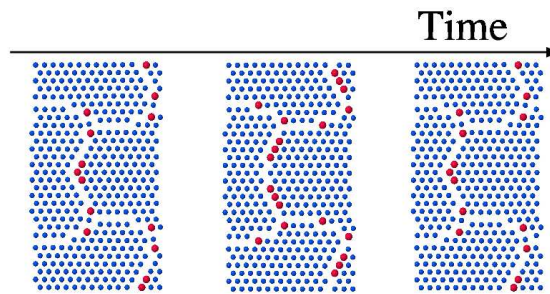


Figure 10: The subharmonic plateau $w/2$ for $\rho = 14/15$, $w = 1/14$, $F = 0.185$. Successive patterns of advancing colloids, separated by intervals of one oscillation period ν^{-1} , illustrating the propagation of an antisoliton in this Shapiro plateau. In a first displacement $10 + 4/2 = 12$ (highlighted) particles jump (the 4 particles crossing oblique antisolitons advance by a half lattice spacing along \hat{x}). Then, at the next period, another $12 + 8/2 = 16$ (highlighted) particles complete the advancement of the string of particles bordering the antisoliton line. At successive periods, the alternating advancement of 12 and 16 particles repeats itself involving successive lines of colloids more and more to the left.

particle number Nw again jumps between a domain and the next: but that takes place in *two* successive oscillation periods instead of one as in the harmonic w step. In the first AC oscillation period $10 + 4/2 = 12$ colloids cross the antisoliton line, whereas the remaining $12 + 8/2 = 16$ jump in the second period. Similarly, in the step leading to the $w/3$ plateau, it takes a sequence of three successive oscillation periods to complete the advancement which transfers Nw particles across the antisoliton. The partial transfers are in this case $10 + 4/2 = 12$, $8 + 4/2 = 10$, and $4 + 4/2 = 6$ particles in period 1, 2 and 3 respectively.

In summary, each Shapiro step is characterized by a periodic advancement pattern during which an integer multiple of Nw particles jump from a commensurate domain to the next. However the m/n -subharmonic step of quantized velocity

$$\frac{v_{\text{cm}}}{\nu a_{\text{las}}} = w \frac{m}{n} \quad (12)$$

is accomplished as a composite of n successive modulation periods, each lasting ν^{-1} , of the AC modulation. After one such complete migration, the entire pattern of positions is displaced bodily by m lattice spacings a_{las} . The subharmonic step leading to $w m/n$ is thus composite, involving n AC modulation periods. The total number mNw of particles that cross the antisoliton is partitioned between the n periods,

$$mNw = \sum_{i=1}^n m_i. \quad (13)$$

The detailed numbers m_i of crossing particles at each individual AC period i will generally depend on ρ , V_0 , Δ_0 , and on the angle between the sliding direction and the antisoliton (soliton) orientation. Occasionally, the partition (13) may even change along a subharmonic step as F increases. We have not found a general analytic rule, if any, determining this partition.

4.1.3. Effect of the corrugation and modulation amplitudes. We now investigate the role played by the corrugation amplitude V_0 and by the modulation amplitude Δ_0 in the formation of Shapiro-step structures as exemplified in the $\rho = 14/15$ mismatched configuration. First of all we remind ourselves that below the pinning threshold corrugation amplitude $V_{0\text{crit}}$ (which, as seen on Fig. 5 is around 0.4 for the present case $\rho = 14/15$) the layer is superlubric, i.e., there is no static friction (other than that, negligible, due to the weak 14/15 commensurability), and a time dependent modulation with amplitude Δ_0 such that $V_0 + \Delta_0 < V_{0\text{crit}}$ would produce no Shapiro steps. Thus we concentrate on corrugation amplitudes above the threshold, where the particle lattice is strongly pinned.

Figure 11 is useful to understand the corrugation dependence of Shapiro steps. We probe three corrugation values: $V_0 = 0.5$, $V_0 = 1$ and $V_0 = 2$ all with an amplitude modulation $\Delta_0 = 70\%V_0$. The whole plateau structure moves to larger forces when the corrugation V_0 is increased. As expected from common sense, the depinning force increases systematically with growing corrugation V_0 , nearly ~ 20 times

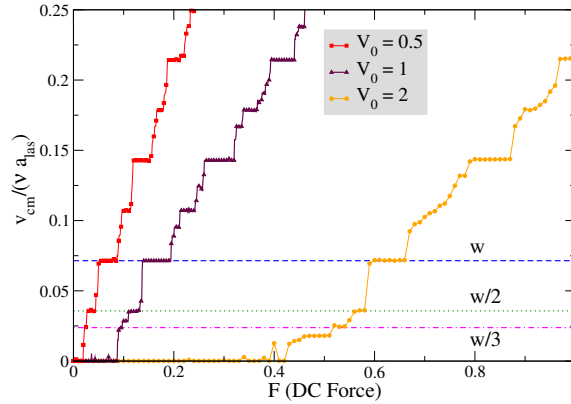


Figure 11: $\rho = 14/15$: rescaled CM velocity for several corrugation amplitudes V_0 , all with a modulation amplitude $\Delta_0 = 70\% V_0$ and frequency $\nu = 0.02$. The initial depinning force F increases rapidly with the corrugation amplitude V_0 . Shapiro steps widen and shift to larger forces when the corrugation is increased.

larger when V_0 changes from 0.5 to 2. With reference to Fig. 5, both $V_0 = 0.5$ and $V_0 = 1$ have $V_0 - \Delta_0 < V_{0\text{crit}}$, thus depinning occurs at an arbitrarily small force, also depending on frequency as discussed below in Sect. 5. In contrast, $V_0 = 2$ has $V_0 - \Delta_0 = 0.6 > V_{0\text{crit}}$, with a broad range of forces for which, independently of frequency, the system remains pinned, thus explaining the huge increase of static friction. The width of the Shapiro steps, especially the smaller ones, also increases with V_0 : for example, the $w/3$ step, barely detectable for $V_0 = 0.5$ and 1, becomes much broader for $V_0 = 2$. In general, a larger potential V_0 amplitude, corresponding to a comparably softer colloid lattice, spatially narrower solitons, and larger static friction, enhances the Shapiro-step structure, which emerges more clearly.

Next, we explore the AC modulation amplitude dependence, Fig. 12, adopting $V_0 = 1$ and varying Δ_0 from 40% V_0 , to $\Delta_0 = 100\% V_0$ (the purple triangles are indeed the same data as the purple triangles of Fig. 11). As in the lattice-matched case Fig. 3, when Δ_0 increases, the Shapiro steps become wider and extend further down to smaller force F . Moreover, a larger AC modulation Δ_0 depresses large- n longer-period subharmonic w/n in favor of shorter ones with smaller n (e.g $w/2$ or w). Conversely, as Fig. 12 shows, all individual plateaus shrink and become more numerous for smaller modulation amplitudes. Moreover, with $\Delta_0 = 40\% V_0$ we detect, in addition to w , $w/2$, $w/3$, and $w/5$, extra fractional plateaus such as $4w/5$, $2w/3$. In short, a small AC modulation amplitude Δ_0/V_0 produces many weak subharmonic steps, while a large modulation promotes fewer stronger and wider ones.

4.2. $\rho = 3/4$

4.2.1. Step structure. There is a clear contrast between the "nearly incommensurate" case, such as $\rho = 14/15$, or $w = 1/14$, and a "strongly commensurate" one, such as $\rho = 3/4$, corresponding to $w = 1/3$, Eq. (10). In this strongly-commensurate case the

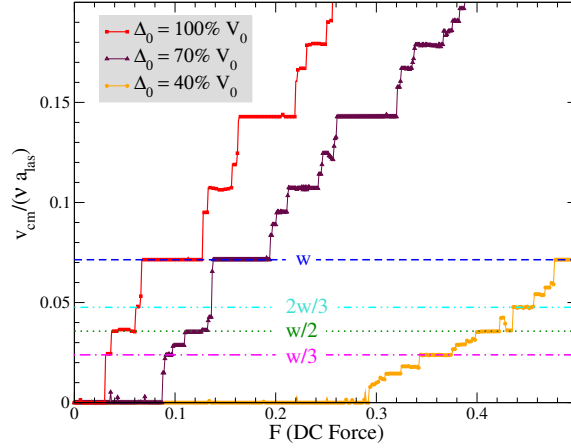


Figure 12: Velocity of the colloid CM (rescaled as in Fig. 2), for $\rho = 14/15$, $T = 0$, oscillation frequency $\nu = 0.02$, corrugation amplitude $V_0 = 1$, for different AC oscillation amplitudes: $\Delta_0 = 40\% V_0$ (dots), $\Delta_0 = 70\% V_0$ (triangles), $\Delta_0 = 100\% V_0$ (squares). Note that the smaller modulation $\Delta_0 = 40\% V_0$ exhibits a richer pattern of steps. The width of the main subharmonic steps tends to increase with increasing modulation amplitude Δ_0 , at the expense of minor steps.

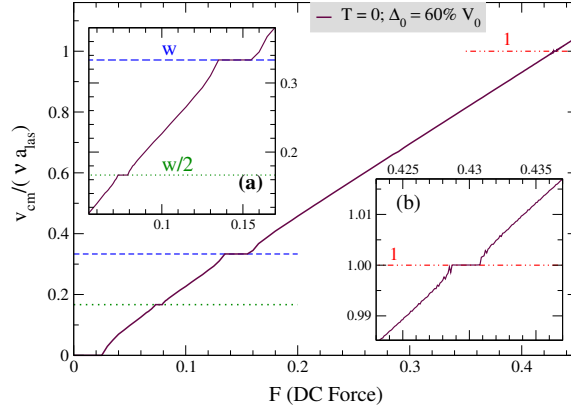


Figure 13: $\rho = 3/4$, $w = 1/3$, $N = 450$ particles, corrugation $V_0 = 1$, modulation $\Delta_0 = 60\% V_0$, oscillation frequency $\nu = 0.02$. Two subharmonic Shapiro steps are visible. Inset (a): Magnified view of the subharmonic plateaus. Inset (b): Magnification of the “trivial” plateau, $v_{\text{cm}}/(\nu a_{\text{las}}) = 1$ representing all colloids advancing as one every modulation period.

Shapiro-step structure – Fig. 13 – shows fewer steps than in the nearly incommensurate case of Fig. 6. Basically only two subharmonic plateaus (w and $w/2$) plus the “trivial” step are detected. Moreover, the width of these plateaus is smaller than it was for $\rho = 14/15$. However, as was the case there, even for strong commensurability $\rho = 3/4$ the plateau widths increase for increasing corrugation amplitude, and that even more rapidly than for $\rho = 14/15$.

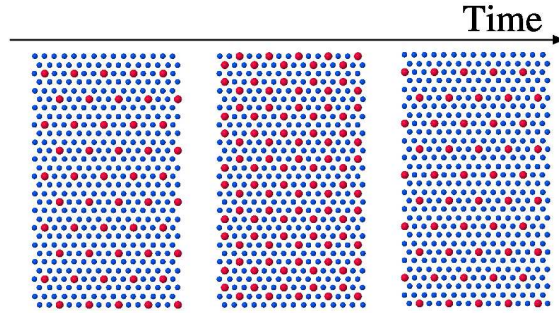


Figure 14: A stroboscopic picture of the $\rho = 3/4$ advancement pattern, similar to Fig. 10, for the $w/2$ step. The antisoliton pattern is so weak that individual hexagonal domains are nearly invisible. The advancing colloids (bolder particles) are highlighted: 150 particles advance in two sets at successive modulation periods: alternately 50 (left), then 100 (center), then again 50 (right), and so on.

4.2.2. Subharmonic advancement of antisolitons. We examine the advancement mechanism for the subharmonic plateaus in Figure 14. The mechanism is again similar to that of Sec. 4.1, Fig. 10. Since $\rho = 3/4$ is further away from unity than $14/15$, the antisoliton pattern is composed by much closer, partly overlapping and less distinct lines. The subdivision in domains is nearly invisible, with each particle always approximately as close to the edge of a domain as to its center. As a result, the oscillations around the average colloid trajectory are far less evident than in Fig. 8. Nevertheless, the advancement mechanics is the same as in the earlier case: e.g. the w/n subharmonic step involves $Nw = 150$ particles, advancing during $n = 2$ periods: we identify a clear pattern of advancing particles, displayed in Fig. 14. Here 150 colloids at the domain boundary advance in a first group of 50 particles in one modulation period, then a second group of 100 in the next period. In the w step, all 150 particles at the boundary cross the antisoliton line at every period: they could be identified by superimposing the highlighted colloids in the first and second panels of Fig. 14.

4.2.3. Thermal effects. Finally we explore thermal effects on the subharmonic step structure. All tests in the $\rho = 14/15$ system show that at finite temperature the fragile Shapiro structure is strongly affected: the steps are washed away by the colloidal diffusive motion. No clear step can be detected for $T > 0.001 \ll T_{\text{room}} = 0.04$, whether the standard $V_0 = 1$ and $\Delta_0 = 60\% V_0$ or other parameters are adopted.

By contrast, with the $\rho = 3/4$ mismatch ratio, where commensurability is stronger, the effects of thermal fluctuations are less dramatic, and at least the strongest steps survive. As shown in Fig. 15, the w plateau persists up to and above T_{room} , the thermal effects leading to a slight reduction in width and to a slight edge rounding compared to $T = 0$. We explored even higher temperature, and found that even at $T = 4T_{\text{room}}$ the w step leaves some remnant of its existence in the force-velocity diagram, Fig. 15a. However, even room-temperature fluctuations are enough to cancel out completely the

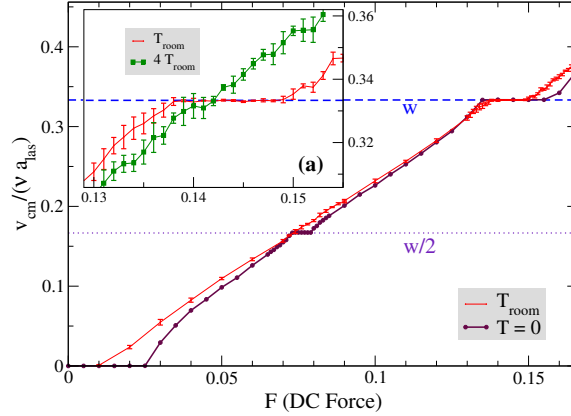


Figure 15: Thermal effects in the $\rho = 3/4$ mismatched configuration, for $V_0 = 1$, $\Delta_0 = 60\% V_0$. Like in Fig. 4, the mean value and error bar of v_{cm} are computed by averaging over several simulations. The w step remains quite well identified at T_{room} , while the $w/2$ step disappears altogether. (a): a zoom-in of the subharmonic w step at $T = T_{\text{room}}$ compared with the much larger temperature $T = 4T_{\text{room}}$ where the plateau structure is washed out by thermal noise.

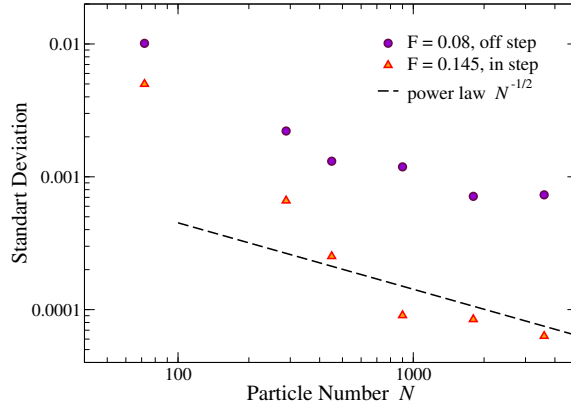


Figure 16: Size scaling of the fluctuations of the CM velocity in room-temperature simulations of the $\rho = 14/15$ mismatched configuration for $V_0 = 1$, $\Delta_0 = 60\% V_0$, executed for $F = 0.08$ (climb between steps) and $F = 0.145$ (step w) of Fig. 15. The various sizes are simulated with rectangular cells similar to the one depicted in Fig. 1. The fluctuations are obtained as the standard deviation evaluated over 4 independent simulations for each size. Dashed line: a $N^{-1/2}$ guide to the eye.

$w/2$ plateau.

Thermal effects on Shapiro steps also depends to some extent on size. As long as the colloid density remains uniform, thermal fluctuations average out for increasing sample size and averaging time: for a given temperature, a larger sample size and longer simulation show flatter, sharper plateaus. Figure 16 shows how the thermal fluctuations on the colloid CM speed depend on the number N of colloids in the simulation supercell. For large size, as expected by statistics, thermal fluctuations scale as $N^{-1/2}$, while when

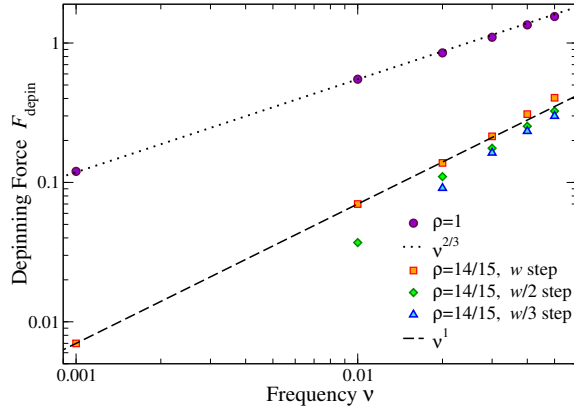


Figure 17: The static depinning force as a function of the modulation frequency in conditions where the sliding barrier vanishes during the modulation period. Circles: the lattice-matched geometry, with $V_0 = 1$, $\Delta_0 = 100\% V_0$. Other symbols: $\rho = 14/15$, with $V_0 = 1$, $\Delta_0 = 70\% V_0$.

the cell lateral size is comparable to or smaller than the correlation length associated to the colloid-colloid interaction, dynamical correlations enhance the fluctuations. Note that inside a plateau (triangles in Fig. 16), the fluctuations are much smaller and the correlation length (marked by the knee in the size scaling) significantly longer, than in a climb between steps.

5. The depinning force

This section deals with the DC-Force – corrugation-amplitude diagram, Fig. 5. We can foresee that, depending on V_0 and Δ_0 , the static-friction force F_{depin} , namely the minimum force required to maintain a net nonzero sliding speed, can fall in one of two alternative regimes. The simplest condition occurs when $V_0 - \Delta_0$ exceeds the Aubry $V_{0\text{crit}}$: then the colloid remains statically pinned throughout the modulation period, with the result that sliding requires a finite driving force greater or equal than the depinning force appropriate to a corrugation $V_0 - \Delta_0$ in the absence of modulation.

Conversely, when $V_0 - \Delta_0 < V_{0\text{crit}}$, for a fraction f_{free} of the oscillation period ν^{-1} , the pinning barrier vanishes, and the colloid slides freely. A slow enough AC modulation gives the particles enough time to take advantage of the temporary lack of pinning and generate the first Shapiro step for arbitrarily small driving force F . In such condition, the depinning force is a function of the modulation frequency. The depinning force F_{depin} can be estimated as follows: During the unpinned time $f_{\text{free}}\nu^{-1}$ the colloids advance at a speed $\simeq \mu F$, where $\mu \simeq \eta^{-1}$ is the colloid mobility; by equating the displacement $f_{\text{free}}\nu^{-1}F\mu$ to a minimum advancement compatible with the overall displacement in the lowest Shapiro step, say $\frac{w}{n}a_{\text{las}}$, we obtain

$$F_{\text{depin}} \simeq \frac{w a_{\text{las}}}{n \mu f_{\text{free}}} \nu. \quad (14)$$

Thus, under modulation conditions such that $V_0 - \Delta_0 < V_{0\text{crit}}$, the static friction force is predicted to vanish linearly with the modulation frequency. Simulations confirm this power law scaling, indicated by the dashed line in Fig. 17. For decreasing frequency, simulations also show that the $n > 1$ subharmonic steps tend to weaken and eventually disappear, see e.g. the diamonds ($w/2$) and triangles ($w/3$) in Fig. 17. As a result, eventually at very low frequency depinning occurs directly into the w step.

The fully-matched case $\rho = 1$ discussed in Sec. 3 has no Aubry transition, so $V_{0\text{crit}} = 0$. Even so, at 100% modulation rate ($\Delta_0 = V_0$), in the brief instants when $\sin(\omega t) \approx -1$, again free sliding is allowed. At finite driving force F a finite time interval $f_{\text{free}}\nu^{-1}$ is compatible with barrier overcoming and consequent free sliding. This interval is obtained by evaluating the region of $F \geq F_{s1}$ using the expression (9) (under the condition $\Delta_0 = V_0$) for the barrier crossing force, obtaining

$$f_{\text{free}} = \frac{1}{2} + \frac{1}{\pi} \arcsin\left(\frac{9Fa_{\text{las}}}{8\pi V_0} - 1\right). \quad (15)$$

By expanding the arcsin function with its argument near -1 (small driving force) we obtain $f_{\text{free}} \simeq [9Fa_{\text{las}}/(4\pi^3 V_0)]^{1/2}$. As above, we then equate the displacement $f_{\text{free}}\nu^{-1}F\mu$ to the minimum advancement required for the colloids to advance by one corrugation lattice spacing, say $\frac{1}{2}a_{\text{las}}$, obtaining

$$F_{\text{depin}} \simeq \pi \left(\frac{V_0 a_{\text{las}}}{9\mu^2}\right)^{1/3} \nu^{2/3}. \quad (16)$$

Again, simulations confirm this result, see Fig. 17, with depinning always occurring into the trivial harmonic step. In principle a similar “critical” $\nu^{2/3}$ power-law regime is to be expected even in the mismatched case $\rho < 1$, under the condition $V_0 - \Delta_0 = V_{0\text{crit}}$ of an instantaneous touching of the free-sliding superlubric Aubry phase during each modulation cycle.

6. Discussion and Conclusion

The present work addresses, by means of MD simulations, the question whether Shapiro step structures can occur in the forced sliding of a 2D colloidal monolayer immersed in an optical lattice spatially periodic corrugation potential whose amplitude has a static DC component plus an AC modulation that oscillates sinusoidally in time. We confirm that Shapiro steps should appear, in the form of intervals of static force within which the CM colloid velocity is quantized, at least at zero temperature, to a value entirely determined by the modulation frequency and by geometric parameters. The only condition required for this to occur at $T = 0$ is that in the absence of the AC modulation the colloids should be pinned by static friction, and not free sliding, as can happen when the 2D colloid lattice and the optical lattice are mismatched and the optical lattice is sufficiently strong. In commensurate, perfectly lattice-matched conditions $\rho = 1$ only “trivial” integer steps are expected, corresponding to the synchronized periodic advancement of all particles at each AC modulation period. In lattice-mismatched conditions $\rho \neq 1$ we find additional

subharmonic Shapiro plateaus beside the integer ones. The crucial quantity governing the subharmonic plateaus is $w = |1 - \rho^{-1}|$, which determines the quantized velocity step value in the totally general form

$$v_{cm} = \nu a_{\text{las}} w \frac{m}{n}, \tag{17}$$

where ν is the AC frequency, a_{las} is the optical lattice spacing, and m and n are small integers. Interestingly, we find that every quantized Shapiro step has a specific real-space signature corresponding to which particles advance synchronously with the AC modulation – a signature which is purely geometric. In a step the total number of advancing particles per modulation period equals exactly a fraction $N w m/n$ of the total particle number N . However, a step corresponding to integer n lasts n periods. During each period ν^{-1} only a sub-fraction of these particles advance by one lattice step, and the total $N w m$ is achieved only at the end of a cycle of n periods.

We analyzed how the corrugation amplitude V_0 and modulation Δ_0 influence the ensuing step structure. An increase in V_0 leads to a comparably softer colloidal layer, thus increased localization and static friction, resulting in a shift to higher forces F of the Shapiro plateaus and generally an increase in their width. On the other hand an increase in Δ_0 to the point of making $V_0 - \Delta_0 < V_{0\text{crit}}$ leads the oscillation to explore more and more of the hard-colloidal-layer region for part of the oscillation period. In this region, free sliding is possible, as well known in the 1D FK model [38]. This results in more extended steps, in particular down to smaller F . In such cases, the smallest (depinning) force is a function of the modulation frequency, and we verified that it changes either as ν as $\nu^{2/3}$ depending on whether a free sliding state is crossed for a finite fraction of the modulation period or just touched instantly. Additionally, a very large $\Delta_0 \simeq V_0$ tends to simplify the rich ladder of subharmonic step structures observed at intermediate Δ_0 .

We also checked how important the specific shape of the corrugation-amplitude time modulation really is for the possibility to observe Shapiro steps. We ran simulations both for the lattice-matched case and for the $\rho = 3/4$ mismatch ratio, replacing $\sin(\omega t)$ in Eq. (7) with a square wave $\text{sign}(\sin(\omega t))$, where $\text{sign}(x)$ equals $x/|x|$ for nonzero x . Compared to the sinusoidal case with identical modulation amplitude Δ_0 and other conditions, the square-wave simulations show quite similar velocity-force profiles, with marginally wider and more robust Shapiro steps. This small difference can be understood as a consequence of the larger RMS modulation of the square wave than the sinusoidal wave for the same peak-to-peak amplitude.

Thermal fluctuations and density inhomogeneities present in real colloid sliding experiments are likely to affect the possibility to observe Shapiro structures. While the perfectly-matched system is barely affected by the thermal Brownian motion, the subharmonic Shapiro-step structures of mismatched systems are far more fragile. Near matching between the colloid and the optical lattice, the loose soliton network is strongly affected by thermal fluctuations, which wash easily away most of the delicate Shapiro plateaus. By contrast, for a more robust (but commensurate) lattice mismatch such as

$\rho = 3/4$, we retrieve subharmonic steps up to T_{room} and even above. We test also the size dependence in the latter case: as long as the density is uniform, a greater number of particles averages out thermal fluctuation, ending up in a flatter and less rounded step.

The model explored in the present work neglects hydrodynamic interactions [53]: while such velocity-dependent many-body forces may affect the quantitative detail of the Shapiro steps, we do not expect they would change the qualitative picture much. In particular, nonuniform solitonic motion, as occurs in mismatched configurations, could be enhanced by hydrodynamic interactions. We are currently investigating this issue in quantitative detail. Also, the detail of the two-body interaction, Eq. (5), is not likely to play any qualitative role in the Shapiro-steps physics. In particular, we expect a similar behavior if the colloid-colloid interaction, rather than screened electrostatic, was the power law describing the repulsion between magnetic colloidal particles in a layer, controlled by a perpendicular magnetic field [54, 55, 56].

In conclusion, this theoretical study predicts that Shapiro-like plateau structures of colloid CM velocities should be easily detected experimentally in a 2D rich geometry— at least in lattice-matched condition, with potential amplitude and oscillation modulation values varying over broad ranges. In mismatched conditions, on the other hand, the experimental detection of subharmonic plateaus seems limited by the ability to provide large regions where the 2D colloid density is constant in space with sufficient accuracy. While experimentally this may not be possible for all subharmonic quantizations, still for a lattice-spacing ratio sufficiently distant from unity, a step structure should be detectable under experimental conditions. Subharmonic steps were indeed detected (although not identified as such) in the simpler 1D experimental setup of Ref. [11].

Acknowledgments

We acknowledge useful discussion with Clemens Bechinger. This work was partly supported under the ERC Advanced Grant No. 320796-MODPHYSFRICT, by the Swiss National Science Foundation through a SINERGIA contract CRSII2_136287, by PRIN/COFIN Contract 2010LLKJBX 004, and by COST Action MP1303.

References

- [1] Ya. I Frenkel and T. A. Kontorova, *Phys. Z. Sowietunion* **13**, 1 (1938).
- [2] T. A. Kontorova and Ya. I. Frenkel, *Zh. Eksp. Teor. Fiz.* **8**, 89 (1938).
- [3] T. A. Kontorova and Ya. I. Frenkel, *Zh. Eksp. Teor. Fiz.* **8**, 1340 (1938).
- [4] L. M. Floría and J. J. Mazo, *Adv. Phys.* **45**, 505 (1996).
- [5] K. Mangold, P. Leiderer, and C. Bechinger, *Phys. Rev. Lett.* **90**, 158302 (2003).
- [6] S. Bleil, H. H. von Grünberg, J. Dobnikar, R. Castañeda-Priego, and C. Bechinger, *Europhys. Lett.* **73**, 450 (2006).
- [7] T. Bohlein, J. Mikhael, and C. Bechinger, *Nat. Mater.* **11**, 126 (2012).
- [8] T. Bohlein and C. Bechinger, *Phys. Rev. Lett.* **109**, 058301 (2012).
- [9] A. Vanossi and E. Tosatti, *Nature Mater.* **11**, 97 (2012).

- [10] A. Vanossi, N. Manini, and E. Tosatti, *P. Natl. Acad. Sci. USA* **109**, 16429 (2012).
- [11] M. P. N. Juniper, A. V. Straube, R. Besseling, D. G. A. L. Aarts, and R. P. A. Dullens, *Nature Commun.* **6**, 7187 (2015).
- [12] S. Shapiro, *Phys. Rev. Lett.* **11**, 80 (1963).
- [13] B. D. Josephson, *Phys. Lett.* **1**, 251 (1962).
- [14] W. C. Stewart, *App. Phys. Lett.* **12**, 277 (1968).
- [15] D. E. McCumber, *J. App. Phys.* **39**, 3113 (1968).
- [16] R. L. Kautz, *Rep. Prog. Phys.* **59**, 935 (1996).
- [17] M. Kvale and S. E. Hebboul, *Phys. Rev. B* **43**, 3720 (1991).
- [18] A. B. Kolton, D. Domínguez, and N. Gronbech-Jensen, *Phys. Rev. Lett.* **86**, 4112 (2001).
- [19] N. Kokubo, R. Besseling, and P. H. Kes, *Phys. Rev. B* **69**, 064504 (2004).
- [20] M. Eichberger, H. Schäfer, M. Krumova, M. Beyer, J. Demsar, H. Berger, G. Moriena, G. Sciaini, and R. J. D. Miller, *Nature* **468**, 799 (2010).
- [21] J. Tekić and B. Hu, *Appl. Phys. Lett.* **95**, 073502 (2009).
- [22] J. Tekić and B. Hu, *Phys. Rev. E* **81**, 036604 (2010).
- [23] J. Tekić and Z. Ivić, *Phys. Rev. E* **83**, 056604 (2011).
- [24] W. Mu, Z. Liu, L. Luan, G. Wang, G. C. Spalding, and J. B. Ketterson, *New J. Phys.* **11**, 103017 (2009).
- [25] P. Mali, J. Tekić, Z. Ivić, and M. Pantić, *Phys. Rev. E* **86**, 046209 (2012).
- [26] A. Libál, C. Reichhardt, Jankó, and C. J. Olson Reichhardt, *Phys. Rev. Lett.* **96**, 188301 (2006).
- [27] M. P. Allen and D. J. Tildesley, *Computer Simulations of Liquids* (Oxford University Press, Oxford, 1991).
- [28] D. R. Nelson and B. I. Halperin, *Phys. Rev. B* **19**, 2457 (1979).
- [29] O. M. Braun and Yu. S. Kivshar, *The Frenkel-Kontorova Model: Concepts, Methods, and Applications* (Springer, Berlin, 2004).
- [30] A. Vanossi and O. M. Braun, *J. Phys.: Condens. Matter* **19**, 305017 (2007).
- [31] D. Mandelli, A. Vanossi, M. Invernizzi, S. V. Paronuzzi Ticco, N. Manini, and E. Tosatti, arXiv:1508.00147, submitted to *Phys. Rev. B* (2015).
- [32] A. D. Novaco and J. P. McTague, *Phys. Rev. Lett.* **38**, 1286 (1977).
- [33] J. P. McTague and A. D. Novaco, *Phys. Rev. B* **19**, 5299 (1979).
- [34] H. Shiba, *J. Phys. Soc. Jpn.* **46**, 1852 (1979).
- [35] H. Shiba, *J. Phys. Soc. Jpn.* **48**, 211 (1980).
- [36] D. Mandelli, A. Vanossi, N. Manini, and E. Tosatti, *Phys. Rev. Lett.* **114**, 108302 (2015).
- [37] S. Aubry and P. Y. Le Daeron, *Physica D* **8**, 381 (1983).
- [38] M. Peyrard and S. Aubry, *J. Phys. C: Solid State Phys.* **16**, 1593 (1983).
- [39] The Aubry transition occurs rigorously only for strictly incommensurate (irrational length ratio f) conditions. In rationally matched situations such as those considered here, the “superlubric” state is characterized by an extremely small nonzero static friction, which vanishes exponentially with the distance from the Aubry point $V_{0\text{crit}}$.
- [40] A. Vanossi, N. Manini, G. Divitini, G. E. Santoro, and E. Tosatti, *Phys. Rev. Lett.* **97**, 056101 (2006).
- [41] N. Manini, A. Vanossi, G. E. Santoro, and E. Tosatti, *Phys. Rev. E* **76**, 046603 (2007).
- [42] N. Manini, M. Cesaratto, G. E. Santoro, E. Tosatti, and A. Vanossi, *J. Phys.: Condens. Matter* **19**, 305016 (2007).
- [43] G. E. Santoro, A. Vanossi, N. Manini, G. Divitini, and E. Tosatti, *Surf. Sci.* **600**, 2726 (2006).
- [44] M. Cesaratto, N. Manini, A. Vanossi, E. Tosatti, and G. E. Santoro, *Surf. Sci.* **601**, 3682 (2007).
- [45] A. Vanossi, G. E. Santoro, N. Manini, M. Cesaratto, and E. Tosatti, *Surf. Sci.* **601**, 3670 (2007).
- [46] A. Vanossi, N. Manini, F. Caruso, G. E. Santoro, and E. Tosatti, *Phys. Rev. Lett.* **99**, 206101 (2007).
- [47] A. Vanossi, G. E. Santoro, N. Manini, E. Tosatti, and O. M. Braun, *Tribol. Int.* **41**, 920 (2008).
- [48] N. Manini, G. E. Santoro, E. Tosatti, and A. Vanossi, *J. Phys.: Condens. Matter* **20**, 224020

- (2008).
- [49] I. E. Castelli, N. Manini, R. Capozza, A. Vanossi, G. E. Santoro, and E. Tosatti, *J. Phys.: Condens. Matter* **20**, 354005 (2008).
 - [50] I. E. Castelli, R. Capozza, A. Vanossi, G. E. Santoro, N. Manini, and E. Tosatti, *J. Chem. Phys.* **131**, 174711 (2009).
 - [51] A. Vigentini, B. Van Hattem, E. Diato, P. Ponzellini, T. Meledina, A. Vanossi, G. Santoro, E. Tosatti, and N. Manini, *Phys. Rev. B* **89**, 094301 (2014).
 - [52] F. Falo, L. M. Floría, P. J. Martinez, and J. J. Mazo, *Phys. Rev. B* **48**, 7434 (1993).
 - [53] H. Diamant, B. Cui, B. Lin, and S. A. Rice, *J. Phys: Cond. Matter* **17**, S2787 (2005).
 - [54] E. L. Bizdoaca, M. Spasova, M. Farle, M. Hilgendorff, and F. Caruso, *J. Magn. Magn. Mater.* **240**, 44 (2002).
 - [55] X. Xu, G. Friedman, K. D. Humfeld, S. A. Majetich, and S. A. Asher, *Chem. Mater.* **14**, 1249 (2002).
 - [56] J. Ge and Y. Yin, *Adv. Mater.* **20**, 3485 (2008).